CRYSTAL GROWTH & DESIGN

pubs.acs.org/crystal

Article

Bulk Crystal Growth and Single-Crystal-to-Single-Crystal Phase Transitions in the Averievite $CsClCu_5V_2O_{10}$

Chao Liu, Chao Ma, Tieyan Chang, Xiaoli Wang, Chuanyan Fan, Lu Han, Feiyu Li, Shanpeng Wang, Yu-Sheng Chen, and Junjie Zhang*

Cite This: *Cryst. Growth Des.* 2024, 24, 9701−9708

Read Online

ACCESS | Metrics & More | Article Recommendations | Supporting Information

ABSTRACT: Quasi-two-dimensional averievites with triangle-Kagome-triangle trilayers are of interest due to their rich structural and magnetic transitions and strong spin frustration that are expected to host a quantum spin liquid ground state with suitable substitution or doping. Herein, we report the growth of bulk single crystals of averievite $CsClCu_5V_2O_{10}$ with dimensions of several millimeters on the edge in order to (1) address the open question of whether the room-temperature crystal structure is $P\bar{3}$ m1, $P\bar{3}$, or $P2_1/c$ or else, (2) to elucidate the nature of phase transitions, and (3) to study direction-dependent physical properties. Single-crystal-to-single-crystal structural transitions at ∼305 and ∼127 K were observed in the averievite $CsClCu_5V_2O_{10}$ single crystals. The nature of the transition at ∼305 K, which was reported as a $P\bar{3}$ m1-$P2_1/c$ transition, was found to be a structural transition from high-temperature $P\bar{3}$ m1 to low-temperature $P\bar{3}$ by combining variable-temperature synchrotron X-ray single crystal and high-resolution powder diffraction. In-plane and out-of-plane magnetic susceptibility and heat capacity measurements confirm a first-order transition at 305 K, a structural transition at 127 K, and an antiferromagnetic transition at 24 K. These averievites are thus ideal model systems for a deeper understanding of structural transitions and magnetism.

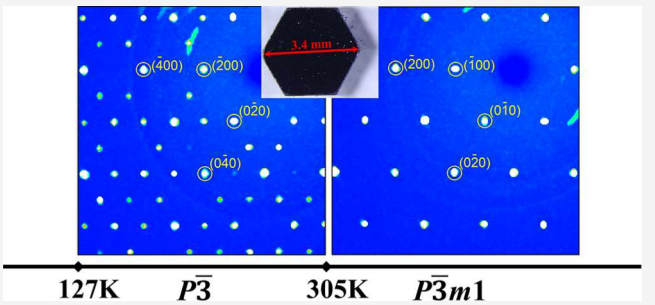

Downloaded via ARGONNE NATL LABORATORY on November 20, 2024 at 15:08:10 (UTC).
See https://pubs.acs.org/sharingguidelines for options on how to legitimately share published articles.

1. INTRODUCTION

Geometrically frustrated systems including triangular, Kagome, and honeycomb lattices have attracted much attention due to the emergence of exotic physical phenomena and many-body quantum states such as quantum spin liquid.[1−4] Among the materials studied, averievite, which represents a class of copper oxide minerals with the formula of $(MX)_nCu_5T_2O_{10}$ (M = K, Rb, Cs, Cu; X = Cl, Br, I; n = 1, 2···; T = P, V), is of current interest.[5−10] Specifically, averievite has a geometrically frustrated quasi-two-dimensional structure consisting of triangle-Kagome-triangle trilayers of Cu^{2+} (S = 1/2).[7,10−12] The ground state of averievites was found to be antiferromagnetic with their Neel temperatures varying from 24 K in $CsClCu_5V_2O_{10}$ (hereafter CCCVO)[7] to 13.6 K in $CsClCu_5P_2O_{10}$[8] (see Table 1). Of particular interest, a series of structural and magnetic transitions under zero field, large anisotropy in in-plane and out-of-plane magnetic properties, and two field-induced transitions under high magnetic field have been discovered in $CsClCu_5P_2O_{10}$ due to the availability of bulk single crystals.[8] The structure of averievite contains Kagome layers, which is a key feature of herbertsmithite $ZnCu_3(OH)_6Cl_2$,[13−16] making averievite very attractive for exploring quantum spin liquid via substitution or doping.[7] Density functional theory calculations predicted that CCCVO and $CsClCu_5P_2O_{10}$ can become quantum spin liquids when nonmagnetic atoms such as Zn completely replace the Cu atoms in the triangle layers.[7,12] Experimentally, the long-range magnetic order has been suppressed to below 2 K based on polycrystalline powders.[7,17,18]

Averievite compounds exhibit rich structure types and complex phase transitions.[9,10] However, to date, certain crystal structures and the underlying mechanism of phase transitions remain controversial. Theoretical calculations based on incorrect crystal structures could mislead experimenters. Furthermore, the existence of ambiguous crystal structures in the literature makes it difficult to understand the structure−property relationship. Six structure types (see Table 1) have been reported in averievite compounds: (i) $P3$ space group with $a_0 = b_0 \sim 6.3$ Å and $c_0 \sim 8.4$ Å;[5] (ii) $P\bar{3}$ $m1$ with $a = b = a_0$ and $c = c_0$;[6−10] (iii) $P\bar{3}$ with $a = b \sim 2a_0$ and $c = c_0$;[9] (iv) $P3m$ with $a = b \sim \sqrt{3}\ a_0$ and $c = c_0$;[6] (v) $P2_1/c$ with $a = c_0$, $b = a_0$, $c \sim \sqrt{3}\ a_0$, and $\beta \sim 90°$;[7] and (vi) $C2/c$ with $a \sim \sqrt{3}\ a_0$, $b = b_0$, $c \sim 2c_0$, and $\beta \sim 95°$.[9,10] Initially, the crystal structure of averievite

Received: August 28, 2024
Revised: November 3, 2024
Accepted: November 4, 2024
Published: November 12, 2024

ACS Publications

© 2024 American Chemical Society

Table 1. Summary of Structural and Magnetic Properties of Averievite[a]

averievites	structure at 296 K	phase transition(s) T (K)	T_N (K)	ref
CCCVO	$P\bar{3}\,m1$ (s)			[6]
	$P2_1/c$ (p)	310, 125 ($P\bar{3}\,m1$ for $T > 310$, $P2_1/c$ for $125 < T < 310$)	24	[7]
	$P\bar{3}$ (s)			[9]
$CsClCu_5P_2O_{10}$	$P\bar{3}\,m1$ (p)	12 ($P\bar{3}\,m1$ for $T > 12$)	3.8	[19]
	$P\bar{3}\,m1$ (s)			[9]
	$P\bar{3}\,m1$ (s)	224 ($P\bar{3}\,m1$ for $T > 224$, $P321$ for $T < 224$)	13.6, 2.18	[8]
$KClCu_5P_2O_{10}$	$C2/c$ (s)			[9]
$KBrCu_5P_2O_{10}$	$C2/c$ (s)			[9]
$RbClCu_5P_2O_{10}$	$C2/c$ (s)			[9]
	$C2/c$ (p)	310 ($P\bar{3}\,m1$ for $T > 310$, $C2/c$ for $T < 310$)	20, 7	[10]
$RbClCu_5V_2O_{10}$	$P3m$ (s)			[6]
$CsBrCu_5P_2O_{10}$	$P\bar{3}\,m1$ (p)	75 ($P2_1/c$ for $T < 75$)	7	[19]
$CsBrCu_5V_2O_{10}$	$P\bar{3}\,m1$ (s)			[6]
$CsICu_5P_2O_{10}$	$P\bar{3}\,m1$ (p)	230 ($P2_1/c$ for $T < 230$)	12.5	[19]
$(CuCl)_2Cu_5V_2O_{10}$	$P\bar{3}\,m1$ (s)			[9]
$(CuCl)Cu_5V_2O_{10}$	$P\bar{3}\,m1$ (p)			[11]
$CuCl_2Cu_5V_2O_{10}$	$P3$ (s)			[5]

[a]Note that s is for single-crystal data, and p is for powder data.

at room temperature was solved and refined using the $P3$ space group based on X-ray diffraction on natural single crystals.[5] In 2009, averievite compounds were first synthesized by Queen and the room-temperature structure was reported to be $P\bar{3}\,m1$ for CCCVO and $CsBrCu_5V_2O_{10}$ and $P3m$ for $RbClCu_5V_2O_{10}$.[6] In 2018, CCCVO was reported to belong to the $P2_1/c$ space group at room temperature based on polycrystalline powders and to undergo a phase transition from $P2_1/c$ to $P\bar{3}\,m1$ at ~310 K on warming.[7] In contrast, Kornyakov et al. reported a $P\bar{3}$ space group at room temperature for CCCVO with a and b doubling referring to the $P\bar{3}\,m1$ structure.[9] Besides CCCVO, the room-temperature structure of $(CuCl)_nCu_5V_2O_{10}$ is also under debate (Table 1), making it difficult to understand the structure−property relationship. On cooling, structural phase transitions have been reported in CCCVO ($P\bar{3}\,m1 \rightarrow P2_1/c$),[7] $CsBrCu_5P_2O_{10}$ ($P\bar{3}\,m1 \rightarrow P2_1/c$),[19] $CsICu_5P_2O_{10}$ ($P\bar{3}\,m1 \rightarrow P321$),[8] and $RbClCu_5P_2O_{10}$ ($P\bar{3}\,m1 \rightarrow C2/c$)[10] on the basis of powder diffraction. Due to the ambiguity of the room-temperature structure, the nature of the structural transitions in averievites remains elusive. Thus, high-resolution synchrotron X-ray single-crystal diffraction is needed to address the above-mentioned fundamental issue. To date, a number of averievite compounds with dimensions of submillimeter on edge have been synthesized in the single-crystal form, including $CsClCu_5P_2O_{10}$ ($0.12 \times 0.12 \times 0.03$ mm^3),[9] CCCVO ($0.06 \times 0.02 \times 0.02$ mm^3 and $0.42 \times 0.40 \times 0.05$ mm^3),[6,9] $RbClCu_5P_2O_{10}$ ($0.21 \times 0.16 \times 0.13$ mm^3),[9] $RbClCu_5V_2O_{10}$ ($0.11 \times 0.04 \times 0.04$ mm^3),[6] $KBrCu_5P_2O_{10}$ ($0.21 \times 0.19 \times 0.06$ mm^3),[9] $CsBrCu_5V_2O_{10}$ ($0.10 \times 0.03 \times 0.03$ mm^3),[6] $KClCu_5P_2O_{10}$ ($0.14 \times 0.10 \times 0.07$ mm^3),[9] and $(Cu_{0.87}Cl_{1.035})_2Cu_5V_2O_{10}$.[9] Bulk single crystals are highly demanded for investigation of direction-dependent physical properties and for understanding the structure−property relationship. Along this line, we have recently reported the bulk growth of $CsClCu_5P_2O_{10}$ single crystals, structural transition, and their direction-dependent magnetic properties.[8]

In this contribution, we reported bulk growth of single crystals of CCCVO using the flux method with $CsCl/CuCl_2$ as the flux for the first time. By a combination of high-resolution synchrotron X-ray single-crystal and powder diffraction techniques, the room-temperature structure of CCCVO was unambiguously determined to be $P\bar{3}$. A structural transition occurs at 305 K on cooling, resulting in a doubling of the cell parameters a and b, and the crystal structure transforms from $P\bar{3}\,m1$ to $P\bar{3}$. Direction-dependent magnetic susceptibility data were collected due to the availability of bulk single crystals. Thermal hysteresis in the out-of-plane magnetic susceptibility around 305 K suggested a first-order structural transition, and a cusp in both in-plane and out-of-plane magnetic susceptibility at 24 K indicates antiferromagnetic ordering. Two anomalies in heat capacity support the structural transition at 127 K and the antiferromagnetic transition at 24 K.

2. RESULTS AND DISCUSSION

2.1. Flux Growth of Bulk Single Crystals. Polycrystalline powders of CCCVO were synthesized using solid-state reactions (see Figure S1) according to the recipe reported by A. S. Botana.[7] In order to check whether CCCVO undergoes congruent or incongruent melting, the as-synthesized polycrystalline powders were heated to 800 °C in air, and the residual materials after heating were checked by using X-ray powder diffraction. It was found that no CCCVO was left and most peaks were indexed to CuO (see Figure S1), indicating that CCCVO undergoes incongruent melting. Thus, melt growth techniques including floating zone, Bridgman, and Czochralski, are not suitable, and the flux method was selected for single-crystal growth.

The first and most difficult step for flux growth is finding a suitable flux.[20−23] Initially, we attempted to grow single crystals of CCCVO using the conditions reported by Queen et al.;[6] however, we failed. We then turned to self-fluxes. The melting points of CsCl and $CuCl_2$ are 645 and 620 °C, respectively. Attempting to grow CCCVO using these two materials separately did not result in CCCVO. We then explored different combinations of CsCl and $CuCl_2$ and found that their mixture in the molar ratio of 1:1 has a low eutectic point of about 420 °C. CuO and V_2O_5 in the molar ratio of 5:1 were added to the $CsCl/CuCl_2$ = 5:5 flux system according to the weight ratio of 1:5, and the cooling procedure was 600−400 °C in 48 h. After the excess flux was dissolved in water, hexagonal and elongated black crystals were obtained (Figure S2). Figure 1a shows a photograph of a typical CCCVO crystal

https://doi.org/10.1021/acs.cgd.4c01195
Cryst. Growth Des. 2024, 24, 9701−9708

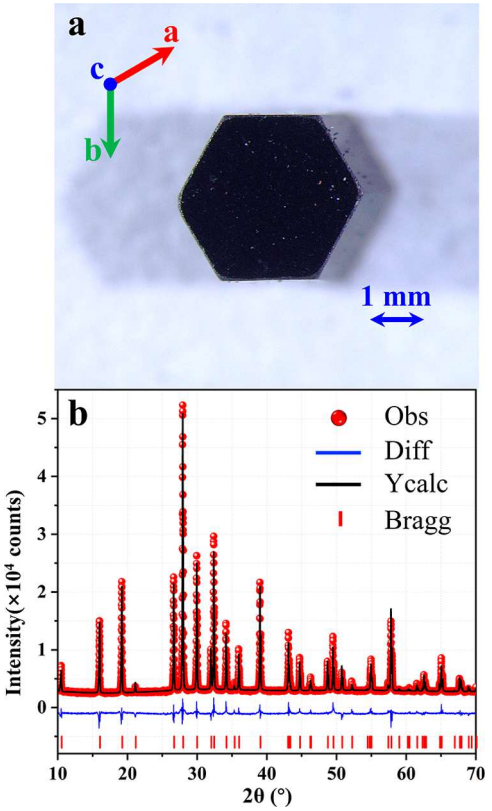

Figure 1. (a) Photo of a typical single crystal of CCCVO from flux growth (3.37 × 2.93 × 0.92 mm^3). (b) In-house X-ray powder diffraction pattern of pulverized single crystals of CCCVO and Rietveld refinement using $P\bar{3}$ $m1$ (λ = 1.5418 Å).

with the crystallographic directions labeled. Figure 1b shows the powder X-ray diffraction data of pulverized hexagonal single crystals. All peaks can be indexed to CCCVO, and no peaks from $Cu_2V_2O_7$ are found. Rietveld refinement using our single-crystal model converged to R_{wp} = 4.07%, R_p = 2.74%, and GOF = 2.30 with lattice parameters of $a = b$ = 6.36690(3) Å and c = 8.37545(6) Å. Our result is in good agreement with the report by Queen et al.[6]

In order to obtain large-size and high-quality single crystals, we optimized the growth conditions, including the raw materials, molar ratio of CsCl to $CuCl_2$, and cooling time. The growth conditions and corresponding results are listed in Table S1. First, we replaced CuO and V_2O_5 with CCCVO polycrystalline powders. Polycrystalline powders are frequently employed as precursors for single-crystal growth of complex compounds by the flux method.[24,25] There is no change in the dimensions of the as-grown single crystals; however, the amount of the secondary phase decreased significantly. Subsequently, in order to further optimize the growth conditions, the $CsCl/CuCl_2$ ratio was adjusted. As the concentration of CsCl increases, the amount of the second phase decreases. At $CsCl/CuCl_2$ = 9:1, the crystal size is up to 1.5 mm, but minor impurity adheres to the crystal surface and is difficult to remove. $CsCl/CuCl_2$ = 7:3 is the best ratio for growing crystals. Finally, the cooling procedure from 600 to 400 °C was optimized to obtain larger single crystals. By extending the cooling time to 96 h, the crystal size increased up to 2.4 mm on the edge and further to 3.4 mm when prolonged to 168 h.

2.2. Structural Transition at ∼305 K. *2.2.1. Single-Crystal X-ray Diffraction at Various Temperatures.* Single-crystal XRD data were collected above and below 305 K to investigate the phase transition previously reported as $P\bar{3}$ $m1$-$P2_1/c$ transition based on powder diffraction.[7] The structures at 400 and 350 K were solved using $P\bar{3}$ m1. As we will discuss later, the superlattice peaks at 296 K were too weak, so we solved the structure using $P\bar{3}$ m1. Figure 2a shows the ball-and-

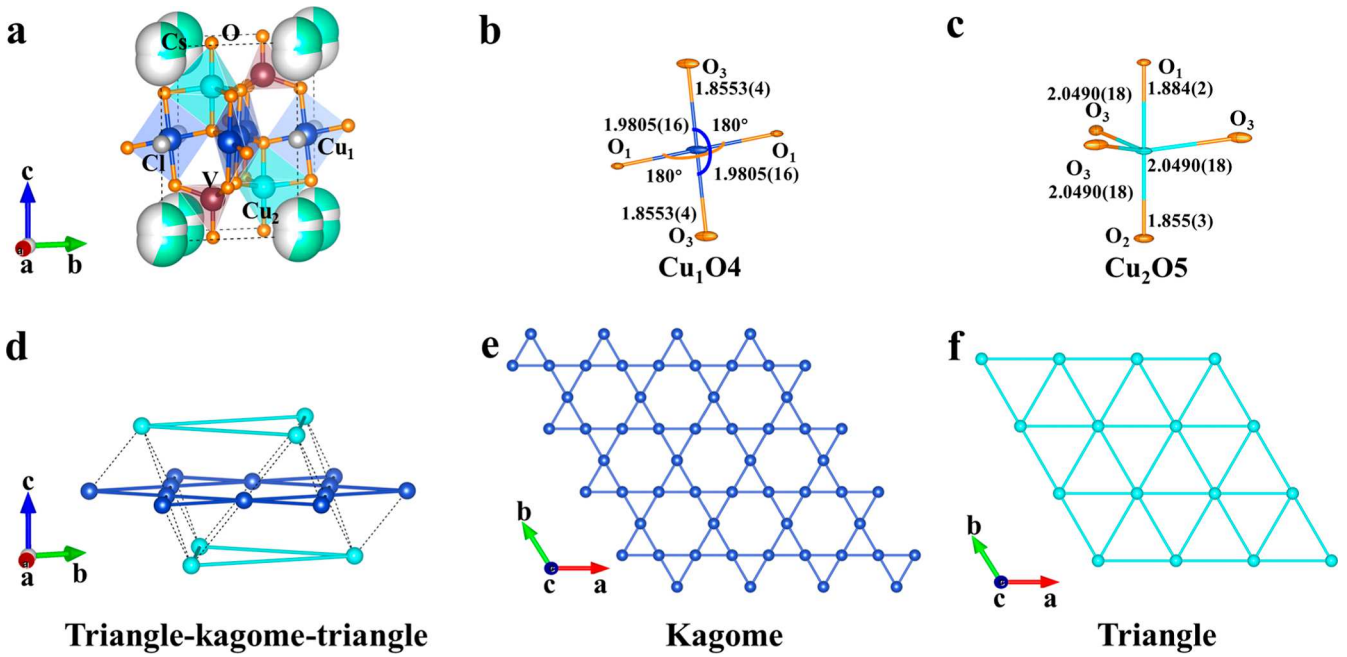

Figure 2. Crystal structure of CCCVO at 350 K. (a) 3D crystal structure viewed along the a axis. (b) Ball-and-stick drawing of the copper oxygen planar environment. (c) Ball-and-stick drawing of copper oxygen polyhedral. (d) Triangle-Kagome-triangle trilayer consisting of copper atoms. (e) Kagome layer consisting of Cu1 atoms. (f) Triangle layer consisting of Cu2 atoms.

https://doi.org/10.1021/acs.cgd.4c01195
Cryst. Growth Des. 2024, 24, 9701−9708

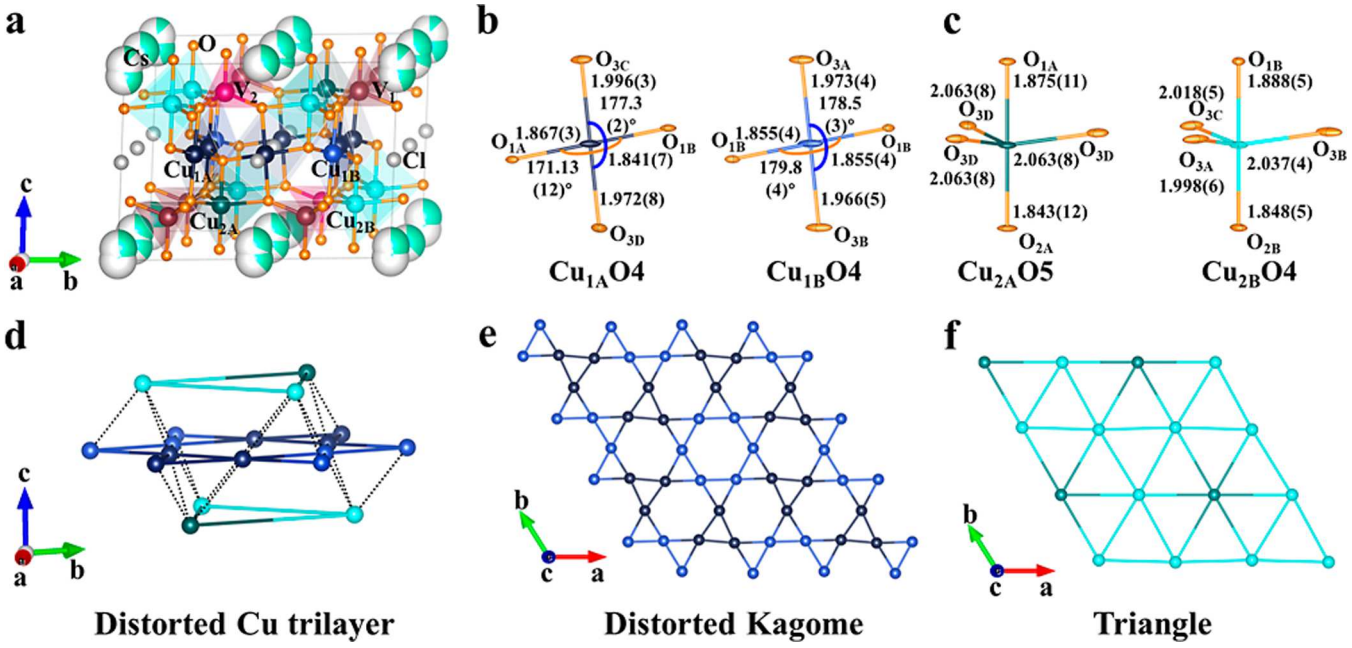

Figure 3. Crystal structure of CCCVO at 200 K. (a) 3D crystal structure viewed along the *a* axis. (b) Ball-and-stick drawings of copper oxygen tetrahedra. (c) Ball-and-stick drawings of copper oxygen polyhedral. (d) Triangle-Kagome-triangle trilayer consisting of copper atoms. (e) Kagome layer consisting of Cu1. (f) Triangle layer consisting of Cu2.

stick model at 350 K. CCCVO belongs to the trigonal space group $P\bar{3}$ m1 with cell parameters of $a = b = 6.3011(1)$ Å, $c = 8.2859(2)$ Å, and $Z = 1$ (see Table S2). The lattice parameters from single-crystal X-ray diffraction are systematically smaller than those from Rietveld refinements (see Table S3), probably due to the zero shift issue in our single-crystal diffraction measurements. The asymmetric unit contains two Cs, one V, two Cu, one Cl, and three oxygen atoms. There are two crystallographic sites for Cu; the first site (Cu1) is bonded to four oxygen atoms with bond lengths of Cu1−O1 = 1.8553(4) Å and Cu1−O3 = 1.9805(16) Å forming a planar environment (see Figure 2b and Table S4). The copper atom (Cu2) at the second site is surrounded by five oxygen atoms with bond lengths of 1.855(3) Å, 1.884(2) Å, and 2.0490(18) Å (see Figure 2c). V is coordinated by four oxygens with a bond length of 1.644(3)−1.7054(18) Å and forms a tetrahedral geometry. Figure 2d−f illustrates the Cu lattice at 350 K (See Table S5). Cu1 atoms form a Kagome layer with a neighboring Cu1−Cu1 distance of 3.15055(6) Å, while Cu2 atoms form two triangular layers with 6.30110(11) Å between adjacent Cu2. The Kagome layer is sandwiched by the two triangular layers with a Cu1−Cu2 distance of 2.8928(4) Å, forming a triangle-Kagome-triangle trilayer. Cs and Cl atoms are filled among trilayers to balance the charge.

Compared with the data at 350 K, apparent superlattice peaks with $\mathbf{Q} = (1/2, 1/2, 0)$ based on the unit cell setting with $a = b \sim 6.28$ Å and $c \sim 8.28$ Å were observed at 200 K (see Figure S3). These superlattice peaks, whose intensities are relatively weak, cannot be indexed using the monoclinic cell ($P2_1/c$ with $a \sim 8.37$ Å, $b \sim 6.36$ Å, $c \sim 11.01$ Å, and $\beta \sim 90.02°$) reported by Botana et al.,[7] suggesting a different structure than $P2_1/c$. Indeed, it belongs to the $P\bar{3}$ space group of the trigonal crystal system with cell parameters of $a = b = 12.5749(3)$ Å, $c = 8.2804(3)$ Å, and $Z = 4$. Figure 3a presents the crystal structure of CCCVO at 200 K. Compared with the high-temperature structure, the O3 site at high temperatures splits into four crystallographic sites at 200 K, and the sites occupied by all other atoms split into two sites; thus, the asymmetric unit consists of four Cs atoms, four Cu atoms, two V atoms, two Cl atoms, and eight O atoms. Figure 3b shows the local environments of the Cu−O polyhedron with bond distances and angles. Notably, the two-dimensional Cu1−O planar environment at high temperatures distorts. Cu2 splits into Cu2A and Cu2B (Figure 3c). V atoms are bonded to four oxygen atoms with bond lengths ranging from 1.650(5) to 1.727(5) Å. Cs and Cl ions fill the voids to realize the charge balance in the system. Figure 3d illustrates the distorted triangle-Kagome-triangle trilayer consisting of Cu at 200 K (see Table S5 for details). The distorted Kagome layer as shown in Figure 3e consists of Cu1A and Cu1B. Within the Kagome layer, the three neighboring Cu1A form an equilateral triangle with a Cu1A-Cu1A distance of 3.171(3) Å, and six neighboring Cu1B form hexatomic rings with a Cu1B−Cu1B distance of 3.1551(14) Å. In addition, the nearest distances between Cu1A and Cu1B are 3.124(3) Å and 3.150(3) Å, respectively, the interior angles of triangle Cu1A-Cu1B−Cu1B are 59.41(7)°, 60.22(8)°, and 60.37(6)°, and the interior angles of a hexagon formed by four Cu1A and two Cu1B are 111.19(8)° × 2, 120.37(6)° × 2, and 128.44(10)° × 2, deviating strongly from 120°. Figure 3f shows the triangular layer formed by Cu2A and Cu2B. Along the *a* direction, there are two arrangements of Cu2: first, Cu2A alternates with Cu2B, and second, all are occupied by Cu2A. Neighboring Cu2A-Cu2A has a distance of 6.284(3) Å, and Cu2A-Cu2B has distances of of 6.1708(15) and 6.4041(15) Å. Our structural model is consistent with Kornyakov et al. at 296 K.[9]

2.2.2. Temperature-Dependent Single-Crystal X-ray Diffraction. Our single-crystal data show different structures between 350 and 200 K. One natural question is at what temperature the phase transition occurs. To address this question, we collected single-crystal diffraction data on cooling from 300 to 105 K. Figure 4 shows the temperature

https://doi.org/10.1021/acs.cgd.4c01195
Cryst. Growth Des. 2024, 24, 9701−9708

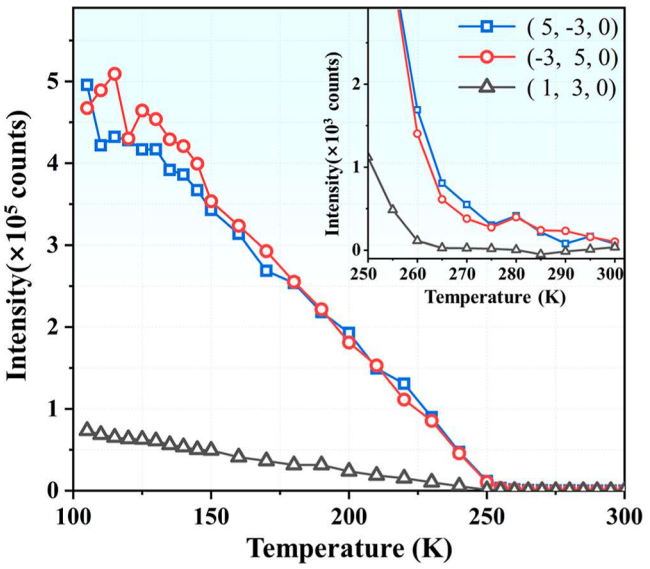

Figure 4. Integrated intensity of (5, −3, 0), (−3, 5, 0), and (1, 3, 0) from synchrotron X-ray single-crystal diffraction based on $P\bar{3}$ as a function of temperature from 300 to 105 K on cooling. Inset: zoom-in between 250 and 300 K.

dependence of three typical peaks indexed and integrated using the 200 K unit cell as a starting point. Two anomalies are observed, the first one at ∼270 K and the second one at ∼127 K, indicating that CCCVO single crystals undergo two successive structural transitions. The transition at ∼270 K is lower than 305 K from magnetic susceptibility data (see below), probably due to the insufficient counting time during data collection. If we increase the statistics, the transition temperature is expected to approach 305 K. By refining data collected at various temperatures, we obtained cell parameters *a*, *c*, and volume as a function of temperature, as shown in Figure S4.

2.2.3. HRPXRD and Rietveld Refinement at Various Temperatures. To verify our single-crystal model, we conducted temperature-dependent high-resolution powder X-ray diffraction at 11-BM at an advanced photon source. Figure 5a presents the high-resolution synchrotron X-ray diffraction data at 400, 295, 200, and 100 K. The patterns at 400 and 295 K look identical. In contrast, additional peaks appear at 200 K compared with 295 K, indicating a structural transition above 200 K. Upon further cooling, more extra peaks show up at 100 K, suggesting another structural phase transition between 200 and 100 K. These high-resolution powder X-ray diffraction data are consistent with our single-crystal results discussed previously. We then carried out Rietveld refinements on the 400 and 200 K data using single-crystal structural models (see Table S3). Figure 5b shows the structural refinement of 400 K data utilizing $P\bar{3}$ m1. The refinement converged to R_{wp} = 9.678% and GOF = 1.87 with lattice parameters of $a = b$ = 6.371681(8) Å and c = 8.378223(6) Å. Figure 5c presents the refinement of 200 K data utilizing $P\bar{3}$, and the refinement converged to R_{wp} = 13.447% and GOF = 2.82 with lattice parameters of $a = b$ = 12.72509(4) Å and c = 8.375747(12) Å. The excellent agreement between calculated and observed

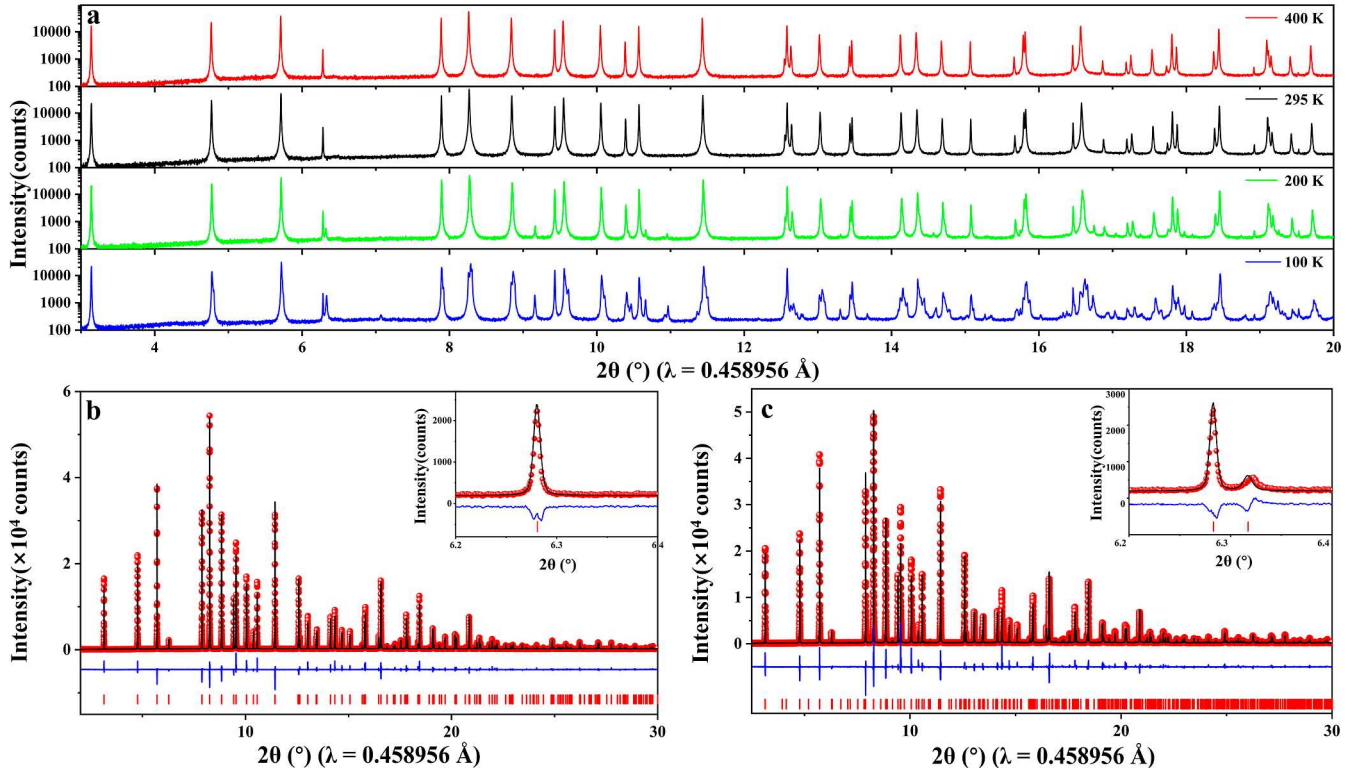

Figure 5. Temperature-dependent high-resolution synchrotron X-ray powder diffraction patterns of CCCVO and Rietveld refinement. (a) Diffraction patterns of CCCVO in the 2θ range of 3−20° at 100, 200, 295, and 400 K. (b) Rietveld refinement on the diffraction data collected at 400 K in the 2θ range of 2−30° using $P\bar{3}$ *m*1. (c) Rietveld refinement on the diffraction data collected at 200 K in the 2θ range of 2−30° using $P\bar{3}$. Red sphere: observed intensity; black line: calculated intensity; blue line: difference between observed and calculated intensities; red bars: Bragg peaks.

https://doi.org/10.1021/acs.cgd.4c01195
Cryst. Growth Des. 2024, 24, 9701−9708

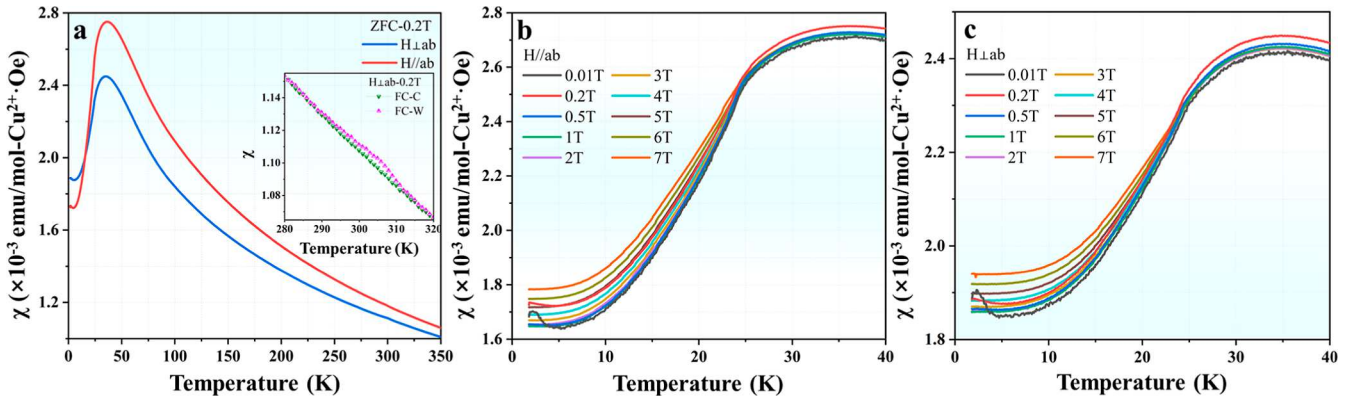

Figure 6. Magnetic susceptibility under various fields. (a) In-plane and out-of-plane magnetic susceptibility under 0.2 T. Inset: magnetic susceptibility in the range of 280−320 K. ZFC: zero field cooling and data collection on warming. (b) Magnetic susceptibility (ZFC data) with magnetic field parallel to the *ab* plane. (c) Magnetic susceptibility (ZFC data) with the magnetic field perpendicular to the *ab* plane.

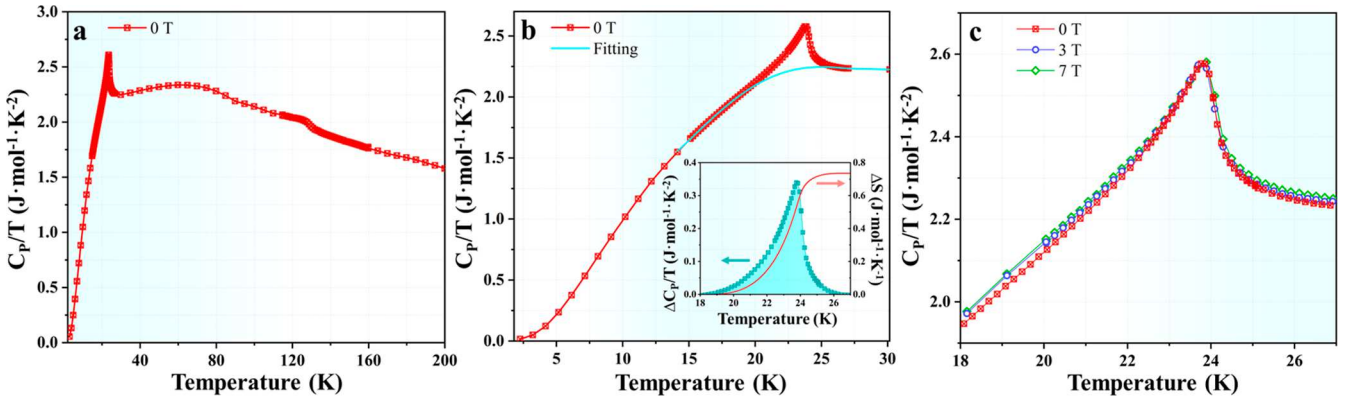

Figure 7. Heat capacity of CCCVO at various fields. (a) Heat capacity of CCCVO in the range of 2−200 K at 0 T. (b) Heat capacity in the range of 2−30 K at 0 T (red square dot line). The cyan line represents the background fit using the fourth-order polynomial. Inset: the cyan point line plot represents the discrepancy between the actual and the fitted background, and the red line represents the integration. (c) Heat capacity as a function of the magnetic field.

intensity at 400 and 200 K corroborates our single-crystal X-ray diffraction results.

2.2.4. Magnetic Susceptibility as a Function of Temperature. Figure 6 presents the temperature-dependent in-plane and out-of-plane magnetic susceptibility data for CCCVO single crystals. Figure 6a (inset) shows a thermal hysteresis in the range of 290−310 K between FC-C and FC-W, suggesting a first-order phase transition at ∼305 K. This is consistent with Botana et al.'s powder data.[7]

2.3. Structural Transition at ∼127 K. Heat capacity data show a clear anomaly at 127 K (Figure 7a). Combining X-ray single-crystal diffraction, powder diffraction, and heat capacity, a structural transition across 127 K occurs. However, we have not obtained a satisfactory structural model for the structure below this transition due to poor single-crystal X-ray diffraction data at 100 K (e.g., twinning and cracking). We tried our best to refine our high-resolution powder diffraction data using structural models reported for averievites in the literature.[7,9,10] We first tried to refine the structure using a single phase. Figures S5−S7 show the Le-Bail fit using $P\bar{3}$, $P2_1/c$, and $C2/c$ as the initial model, and the refinements converged to R_{wp} = 29.73%, 28.33%, and 29.66%, respectively. As can be seen, none of them is satisfactory. Because 100 K is very close to the transition temperature, it is likely that the 100 K data consist of multiple phases. Thus, $P\bar{3}$ and $P2_1/c$, $P\bar{3}$ and $C2/c$ were used as initial models (see Figures S8−S9), and the fit converged to R_{wp} = 30.22% and 27.72%, respectively. Therefore, synchrotron X-ray single-crystal diffraction at a low temperature of less than 100 K is needed to address this puzzle.

2.4. Antiferromagnetic Transition at ∼24 K. *2.4.1. Magnetic Susceptibility and Magnetization.* The successful growth of bulk single crystals promotes the investigation of direction-dependent physical properties. Figure 6a shows the magnetic susceptibility of CCCVO under 0.2 T with a magnetic field parallel/perpendicular to the *ab* plane. The two curves do not overlap, indicating anisotropic magnetic properties. The first derivatives of ZFC (Figure S10) show a maximum at 24 K, indicating a phase transition. The transition temperature is consistent with Botana et al.[7] Figure 6b,c presents the temperature-dependent magnetic susceptibility (ZFC) at various magnetic fields between 1.8 and 40 K. The cusp shape at 24 K and obvious response to the external magnetic field suggest an antiferromagnetic transition. Figure S11 presents the Curie−Weiss fit in the temperature range of 150−275 K with H//ab; an effective moment of μ_{eff} = 2.09 μ_B and a Weiss temperature of θ_{CW} = −161 K are obtained. Figure S12 presents the Curie−Weiss fit with H⊥ab; an effective moment of μ_{eff} = 2.13 μ_B and Weiss temperature of θ_{CW} = −213 K are obtained. The effective magnetic moments are close to the expected value of 1.73 μ_B for the Cu ions with S = 1/2,[26] and the negative and large values of the Weiss temperatures indicate a strong antiferromagnetic interaction

https://doi.org/10.1021/acs.cgd.4c01195
Cryst. Growth Des. 2024, 24, 9701−9708

in the system. Magnetization data as a function of magnetic fields are shown in Figures S13 and S14.

2.4.2. Heat Capacity. Figure 7 shows the specific heat of a CCCVO single crystal at various magnetic fields. The λ-type peak at 24 K (see Figure 7b), which is obtained from the peak of the first-order derivative of the magnetic susceptibility (see Figure S10), suggests a second-order phase transition. The specific heat background was fitted with a fourth-order polynomial, and the specific heat difference and integration are shown in the inset of Figure 7b. The entropy change associated with the magnetic order is estimated to be ΔS = 0.78 (J/mol K), which is only 2.7% of the expected three-dimensional antiferromagnetic transition of 5*Rln2. The tiny magnetic entropy release can be understood. In the structure of $CsClCu_5V_2O_{10}$, the magnetic Cu^{2+} ions form a strongly frustrated triangle and Kagome lattice (see Figure 3). Even below 24 K, only a small portion of spins develop antiferromagnetic order; most spins are still highly frustrated. The heat capacity data under different applied magnetic fields are shown in Figure 7c, where the peaks overlap, indicating that a larger magnetic field is needed to suppress the transition.

3. CONCLUSIONS

We report the successful growth of bulk single crystals of CCCVO using the flux method. The structure at room temperature was determined to be $P\bar{3}m1$. By combining variable-temperature high-resolution synchrotron X-ray single crystals and powder diffraction, two first-order structural transitions (one at ~305 K and the other at ~127 K) were observed. The structure between 305 and 200 K was unambiguously solved using $P\bar{3}$ by synchrotron X-ray single-crystal diffraction. The triangle-Kagome-triangle trilayer structure, composed of Cu^{2+}, is strongly distorted on cooling. Our experiments have resolved the long-standing controversy of the room-temperature crystal structure of averievite and the nature of phase transition across ~305 K. Direction-dependent magnetic susceptibility measurements show two anomalies: one between 290 and 310 K corresponding to a structural transition and another one at 24 K which corresponds to antiferromagnetic ordering. Heat capacity shows two anomalies: one at 127 K and the other one at 24 K. The preparation of large CCCVO crystals serves as a template for growing other averievite single crystals, including quantum spin liquids candidates such as $CsClCu_3Zn_2V_2O_{10}$ and $CsClCu_3Zn_2Ti_2O_{10}$.[7] Our results not only reveal the nature of structural transitions and anisotropic magnetic properties in the averievite $CsClCu_5V_2O_{10}$ but also call for more systematic studies in this class of materials.

■ ASSOCIATED CONTENT

Supporting Information

The Supporting Information is available free of charge at https://pubs.acs.org/doi/10.1021/acs.cgd.4c01195.

Experimental details (polycrystalline synthesis, single-crystal growth, X-ray powder diffraction, X-ray single-crystal diffraction, magnetic susceptibility, magnetization, and heat capacity); tables of growth conditions, crystallographic data, bond length, and angles; and figures of powder diffraction and single-crystal diffraction, Rietveld refinements using various models, Curie–Weiss fits, and in-plane and out-of-plane magnetization as a function of magnetic field (PDF)

Accession Codes

Deposition numbers 2264549, 2264551, 2264817, and 2338862 contain the supplementary crystallographic data for this paper. These data can be obtained free of charge via the joint Cambridge Crystallographic Data Centre (CCDC) and Fachinformationszentrum Karlsruhe Accessstructuresservice.

■ AUTHOR INFORMATION

Corresponding Author

Junjie Zhang − *Institute of Crystal Materials, State Key Laboratory of Crystal Materials, Shandong University, Jinan, Shandong 250100, China;* orcid.org/0000-0002-5561-1330; Email: junjie@sdu.edu.cn

Authors

Chao Liu − *Institute of Crystal Materials, State Key Laboratory of Crystal Materials, Shandong University, Jinan, Shandong 250100, China*

Chao Ma − *Institute of Crystal Materials, State Key Laboratory of Crystal Materials, Shandong University, Jinan, Shandong 250100, China*

Tieyan Chang − *NSF's ChemMatCARS, The University of Chicago, Lemont, Illinois 60439, United States;* orcid.org/0000-0002-7434-3714

Xiaoli Wang − *Institute of Crystal Materials, State Key Laboratory of Crystal Materials, Shandong University, Jinan, Shandong 250100, China*

Chuanyan Fan − *Institute of Crystal Materials, State Key Laboratory of Crystal Materials, Shandong University, Jinan, Shandong 250100, China*

Lu Han − *Institute of Crystal Materials, State Key Laboratory of Crystal Materials, Shandong University, Jinan, Shandong 250100, China*

Feiyu Li − *Institute of Crystal Materials, State Key Laboratory of Crystal Materials, Shandong University, Jinan, Shandong 250100, China*

Shanpeng Wang − *Institute of Crystal Materials, State Key Laboratory of Crystal Materials, Shandong University, Jinan, Shandong 250100, China;* orcid.org/0000-0003-2166-0043

Yu-Sheng Chen − *NSF's ChemMatCARS, The University of Chicago, Lemont, Illinois 60439, United States*

Complete contact information is available at: https://pubs.acs.org/10.1021/acs.cgd.4c01195

Notes

The authors declare no competing financial interest.

■ ACKNOWLEDGMENTS

J.Z. thanks Prof. Xutang Tao from Shandong University for providing valuable support and fruitful discussions. Work at Shandong University was supported by the National Natural Science Foundation of China (grant nos. 12374457 and 12074219), the Taishan Scholars Program of Shandong Province (grant no. tsqn201909031), the QiLu Young Scholars Program of Shandong University, the Crystalline Materials and Industrialization Joint Innovation Laboratory of Shandong University and Shandong Institutes of Industrial Technology (grant no. Z1250020003), and the Project for Scientific Research Innovation Team of Young Scholars in Colleges and Universities of Shandong Province (grant no. 2021KJ093). NSF's ChemMatCARS, Sector 15, at the Advanced Photon Source (APS), Argonne National Laboratory (ANL), is

supported by the Divisions of Chemistry (CHE) and Materials Research (DMR), National Science Foundation, under grant numbers NSF/CHE-1834750 and 2335833. This research used resources of the Advanced Photon Source, a U.S. Department of Energy (DOE) Office of Science user facility operated for the DOE Office of Science by the Argonne National Laboratory under contract no. DE-AC02-06CH11357.

REFERENCES

(1) Pavarini, E.; Koch, E.; Coleman, P. *Many-body Physics: From Kondo to Hubbard*; Forschungszentrum Jülich GmbH Institute for Advanced Simulation, 2015.
(2) Lancaster, T. Quantum spin liquids. *Contemp. Phys.* **2023**, *64* (2), 127−146.
(3) Balents, L. Spin liquids in frustrated magnets. *Nature* **2010**, *464*, 199−208.
(4) Zhou, Y.; Kanoda, K.; Ng, T.-K. Quantum spin liquid states. *Rev. Mod. Phys.* **2017**, *89* (2), 025003.
(5) Starova, G. L.; Krivovlchev, S. V.; Fundamensky, V. S.; Filatov, S. K. The crystal structure of averievite, $Cu_5O_2(VO_4)_2$·nMX: comparison with related compounds. *Mineral. Mag.* **1997**, *61* (406), 441−446.
(6) Queen, W. *Synthesis and Characterization of Magnetic Solids Containing Periodic Arrays of Transition Metal Oxide Nanostructures*; Clemson University, 2009.
(7) Botana, A. S.; Zheng, H.; Lapidus, S. H.; Mitchell, J. F.; Norman, M. R. Averievite: A copper oxide kagome antiferromagnet. *Phys. Rev. B* **2018**, *98* (5), 054421.
(8) Liu, C.; Chang, T.; Wang, S.; Zhou, S.; Wang, X.; Fan, C.; Han, L.; Li, F.; Ren, H.; Wang, S.; Chen, Y.; Zhang, J. Cascade of Phase Transitions and Large Magnetic Anisotropy in a Triangle-Kagome-Triangle Trilayer Antiferromagnet. *Chem. Mater.* **2024**, *36* (19), 9516−9525.
(9) Kornyakov, I. V.; Vladimirova, V. A.; Siidra, O. I.; Krivovichev, S. V. Expanding the Averievite Family, $(MX)Cu_5O_2(T^{5+}O_4)_2$ (T^{5+} = P, V; M = K, Rb, Cs, Cu; X = Cl, Br): Synthesis and Single-Crystal X-ray Diffraction Study. *Molecules* **2021**, *26* (7), 1833.
(10) Mohanty, S.; Babu, J.; Furukawa, Y.; Nath, R. Structural and double magnetic transitions in the frustrated spin-1/2 capped-kagome antiferromagnet $(RbCl)Cu_5P_2O_{10}$. *Phys. Rev. B* **2023**, *108* (10), 104424.
(11) Ginga, V. A.; Siidra, O. I.; Firsova, V. A.; Charkin, D. O.; Ugolkov, V. L. Phase evolution and temperature-dependent behavior of averievite, $Cu_5O_2(VO_4)_2(CuCl)$ and yaroshevskite, $Cu_9O_2(VO_4)_4Cl_2$. *Phys. Chem. Miner.* **2022**, *49* (9), 38.
(12) Dey, D.; Botana, A. S. Role of chemical pressure on the electronic and magnetic properties of the spin-1/2 kagome mineral averievite. *Phys. Rev. B* **2020**, *102* (12), 125106.
(13) Shores, M. P.; Nytko, E. A.; Bartlett, B. M.; Nocera, D. G. A Structurally Perfect S = 1/2 Kagomé Antiferromagnet. *J. Am. Chem. Soc.* **2005**, *127* (39), 13462−13463.
(14) Helton, J. S.; Matan, K.; Shores, M. P.; Nytko, E. A.; Bartlett, B. M.; Yoshida, Y.; Takano, Y.; Suslov, A.; Qiu, Y.; Chung, J. H.; et al. Spin Dynamics of the Spin-1/2Kagome Lattice Antiferromagnet $ZnCu_3(OH)_6Cl_2$. *Phys. Rev. L.* **2007**, *98* (10), 107204.
(15) Freedman, D. E.; Han, T. H.; Prodi, A.; Müller, P.; Huang, Q.-Z.; Chen, Y.-S.; Webb, S. M.; Lee, Y. S.; McQueen, T. M.; Nocera, D. G. Site Specific X-ray Anomalous Dispersion of the Geometrically Frustrated Kagomé Magnet, Herbertsmithite, $ZnCu_3(OH)_6Cl_2$. *J. Am. Chem. Soc.* **2010**, *132* (45), 16185−16190.
(16) Norman, M. R. Colloquium: Herbertsmithite and the search for the quantum spin liquid. *Rev. Mod. Phys.* **2016**, *88* (4), 041002.
(17) Biesner, T.; Roh, S.; Pustogow, A.; Zheng, H.; Mitchell, J. F.; Dressel, M. Magnetic terahertz resonances above the Néel temperature in the frustrated kagome antiferromagnet averievite. *Phys. Rev. B* **2022**, *105* (6), L060410.
(18) Georgopoulou, M.; Boldrin, D.; Fåk, B.; Manuel, P.; Gibbs, A.; Ollivier, J.; Suard, E.; Wills, A. S. Magnetic ground states and excitations in Zn-doped averieite—a family of oxide-based S = 1/2 kagome antiferromagnets. Preprint at http://arxiv.org/abs/2306.14739, accessed 11/9/2024.
(19) Winiarski, M. J.; Tran, T. T.; Chamorro, J. R.; McQueen, T. M. $(CsX)Cu_5O_2(PO_4)_2$ (X = Cl, Br, I): A Family of Cu^{2+} S = 1/2 Compounds with Capped-Kagomé Networks Composed of OCu4 Units. *Inorg. Chem.* **2019**, *58* (7), 4328−4336.
(20) Elwell, D.; Neate, B. W. Mechanisms of crystal growth from fluxed melts. *J. Mater. Sci.* **1971**, *6* (12), 1499−1519.
(21) Bugaris, D. E.; zur Loye, H. Materials Discovery by Flux Crystal Growth: Quaternary and Higher Order Oxides. *Angew. Chem., Int. Ed.* **2012**, *51* (16), 3780−3811.
(22) Juillerat, C. A.; Klepov, V. V.; Morrison, G.; Pace, K. A.; zur Loye, H.-C. Flux crystal growth: a versatile technique to reveal the crystal chemistry of complex uranium oxides. *Dalton Trans.* **2019**, *48* (10), 3162−3181.
(23) Klepov, V. V.; Juillerat, C. A.; Pace, K. A.; Morrison, G.; zur Loye, H.-C. Soft" Alkali Bromide and Iodide Fluxes for Crystal Growth. *Front. Chem.* **2020**, *8*, 518.
(24) Kawano, T.; Yamane, H. Synthesis Crystal Structure Analysis, and Photoluminescence of Ti4+-Doped $Mg_5SnB_2O_{10}$. *Chem. Mater.* **2010**, *22* (21), 5937−5944.
(25) Zhao, B.; Bai, L.; Li, B.; Zhao, S.; Shen, Y.; Li, X.; Ding, Q.; Ji, C.; Lin, Z.; Luo, J. Crystal Growth and Optical Properties of Beryllium-Free Nonlinear Optical Crystal $K_3Ba_3Li_2Al_4B_6O_{20}F$. *Cryst. Growth Des.* **2018**, *18* (2), 1168−1172.
(26) Mugiraneza, S.; Hallas, A. M. Tutorial: a beginner's guide to interpreting magnetic susceptibility data with the Curie-Weiss law. *Commun. Phys.* **2022**, *5* (1), 95.

https://doi.org/10.1021/acs.cgd.4c01195
Cryst. Growth Des. 2024, 24, 9701−9708